

Hai-Feng GAO
Anjenq WANG
Enrico ZIO
Wei MA

FATIGUE STRENGTH RELIABILITY ASSESSMENT OF TURBO-FAN BLADES BY KRIGING-BASED DISTRIBUTED COLLABORATIVE RESPONSE SURFACE METHOD

OCENA NIEZAWODNOŚCI WYTRZYMAŁOŚCI ZMĘCZENIOWEJ ŁOPATEK TURBOWENTYLATORA ROZPROSZONĄ METODĄ POWIERZCHNI ODPOWIEDZI Z WYKORZYSTANIEM KRIGINGU

Fatigue crack propagation affects the operational reliability of engine turbo-fan blades. In this article, we integrate a Kriging regression model and a distributed collaborative response surface method (DCRSM) for the reliability assessment of turbo-fan blades, considering the relevant uncertainty. Following a series of deterministic analyses, such as steady-state aerodynamic analysis, harmonic response analysis and Campbell diagram, and based on the assumption that vibration stress is mainly from aerodynamic load, the fatigue strength is calculated for turbo-fan blades under coupling aerodynamic forces, according to a modified Goodman curve of titanium-alloy. Giving consideration to the uncertainty of the resonance frequencies and material properties, the fatigue strength of the turbo-fan blade is evaluated, including probabilistic analysis and sensitivity analysis. In the case study analyzed, the conclusions are that the fatigue strength reliability reaches 96.808% with confidence level of 0.95 for the turbo-fan blade under the coupling aerodynamic forces, and the first three-order resonant frequencies are found to have important influence on the fatigue performance of turbo-fan blades.

Keywords: turbo-fan blade, fatigue strength, reliability assessment, Kriging, distributed collaborative response surface method.

Propagacja pęknięć zmęczeniowych wpływa na niezawodność pracy łopatek turbowentylatora w silnikach samolotowych. W przedstawionej pracy, niezawodność łopatek turbo-wentylatora oceniano za pomocą techniki która łączy rozproszoną metodę powierzchni odpowiedzi (ang. distributed collaborative response surface method, DCRSM) z krigingiem, z jednoczesnym uwzględnieniem niepewności. Po przeprowadzeniu serii analiz deterministycznych, w tym analizy aerodynamicznej w stanie ustalonym, analizy harmonicznej i wyznaczeniu wykresu Campbella, oraz przyjmując założenie, że naprężenia wibracyjne powstają głównie na skutek obciążeń aerodynamicznych, obliczono wytrzymałość zmęczeniową łopatek turbowentylatora w warunkach sprzęgających sił aerodynamicznych, zgodnie ze zmodyfikowaną krzywą Goodmana dla stopu tytanu. Biorąc pod uwagę niepewność częstotliwości rezonansowych i właściwości materiału, wytrzymałość zmęczeniową łopatki turbowentylatora określano na podstawie analizy probabilistycznej i analizy czułości. W omawianym studium przypadku wykazano, że niezawodność wytrzymałości zmęczeniowej łopatki turbowentylatora w warunkach sprzęgających sił aerodynamicznych sięga 96,808% przy poziomie ufności 0,95, a trzy pierwsze postacie drgań rezonansowych mają istotny wpływ na jej wydajność zmęczeniową.

Słowa kluczowe: łopatka turbowentylatora, wytrzymałość zmęczeniowa, ocena niezawodności, kriging, rozproszona metoda powierzchni odpowiedzi.

Acronyms

MCM	Monte Carlo method.
DCRSM	Distributed collaborative response surface method.
DCRSF	Distributed collaborative response surface function.
Kriging-based DCRSM	Kriging-based distributed collaborative response surface method.
Kriging-based DCRSF	Kriging-based distributed collaborative response surface function.

Notation

E	Elastic modulus	P	Density
μ	Poisson ratio	σ_m	Average stress

$\sigma_{es,max}$	Maximum equivalent stress	σ_a	Stress amplitude
$\sigma_{vs,max}$	Maximum vibration stress	$\hat{\sigma}_a$	Maximum vibration stress
$f1$	First-order frequency	$f2$	Second-order frequency
$f3$	Third-order frequency	\hat{P}_f	Failure probability
α_{y_i}	Sensitivity coefficient	R	Structural reliability

1. Introduction

Turbo-fan blades are important rotational parts which play an important role in conveying air into the inside and outside lanes of aeroengines. Fan blades with wide span-chord ratio suffer from high stress level and severe working conditions, and are susceptible to vibration, due to the centrifugal force produced by high rotation speed and the aerodynamic force caused by the airflow. In addition, vibration, especially resonance, can produce great stress and easily result in blade fatigue failure. Therefore, fatigue strength analysis is the key to study the fatigue resistance problems of blades, and is necessary to ensure the stability and reliability of engines during flight [21].

Recently, many researchers have studied some engine blade high-cycle fatigue strength issues through computational/experimental methods. Poursaeidi et al. [16] analyzed the influence of natural frequencies on compressor blade failure, considering centrifugal forces and simplified aerodynamic loads. Srinivasan [20] summarized the vibration problems of turbine blades. Xu et al. [24] carried out some studies about the vibration and stress of an axial fan blade under centrifugal forces and aerodynamic loads through finite element and experiment methods. The efforts focus on deterministic analyses on the vibration and fatigue strength of gas engine blades. However, the relevant uncertainties should be carefully considered for accurate vibration characteristics prediction and reliability analysis of turbo-fan blades.

Accurate and efficient numerical simulation methods are crucial for the fatigue strength prediction of complex mechanical structures. Probabilistic methods mainly include first-order reliability method (FORM) [4, 13, 17], second-order reliability method (SORM) [6, 22], response surface method (RSM) [3, 5, 18] and Monte Carlo method (MCM) [1, 2, 25, 26, 27]. A main practical difference among the simulation methods is the computational accuracy and efficiency. In order to ensure the numerical accuracy and computational efficiency, in this paper, we integrate the Kriging and distributed collaborative response surface method (DCRSM) [7, 10] and propose Kriging-based DCRSM for the fatigue strength assessment of turbo-fan blades, considering relevant uncertainties.

The Kriging-based distributed collaborative reliability approach is proposed in Section 2. Section 3 presents the deterministic numerical analysis of the vibration performance and fatigue strength of aeroengine turbo-fan blades and presents a reliability assessment framework by Kriging-based DCRSM. The probabilistic analysis on the vibration performance and fatigue strength with sensitivity analyses is completed in Section 4. Section 5 discusses the conclusions of the work.

2. Kriging-based DCRSM reliability assessment framework

2.1. Kriging

Kriging is an interpolation approach based on the assumption that there is a spatial correlation between the values of the function to be approximated [23]. At present, Kriging is a representative approxima-

tion method to construct surrogate models, which are widely used for structural reliability analysis.

For a set of p' design sites $\mathbf{X}=[\mathbf{x}_1, \mathbf{x}_2, \dots, \mathbf{x}_n]$ with $\mathbf{x}_k \in R^p$ and response $\mathbf{Y}=[y_1, y_2, \dots, y_m]$ with $y_d \in R^p$, we take model \hat{y} to express deterministic response $y(\mathbf{x})$, which can be formulated as the sum of the regression model F and the random function $z(\mathbf{x})$ [19]:

$$\hat{y}_l(\mathbf{x}) = F(\beta_{:,l}, \mathbf{x}) + z_l(\mathbf{x}), \quad l = 1, 2, \dots, q \quad (1)$$

$$\begin{aligned} \mathcal{F}(\beta_{:,l}, \mathbf{x}) &= \beta_{1,l}f_1(\mathbf{x}) + \beta_{2,l}f_2(\mathbf{x}) + \dots + \beta_{t,l}f_t(\mathbf{x}) \\ &= [f_1(\mathbf{x}), f_2(\mathbf{x}), \dots, f_t(\mathbf{x})]\beta_{:,l} \\ &= \mathbf{f}(\mathbf{x})^T \beta_{:,l} \end{aligned} \quad (2)$$

where the coefficient $\beta_{:,l}$ is a regression parameter to be estimated based on data. In the current paper, a regression model with second-order polynomial is adopted, as follows:

$$\begin{cases} \mathbf{f}(\mathbf{x}) = [f_1(\mathbf{x}), f_2(\mathbf{x}), \dots, f_{p+1}(\mathbf{x}), f_{p+2}(\mathbf{x}), \dots, f_{2p+1}(\mathbf{x}), f_{2p+2}(\mathbf{x}), \dots, f_{3p}(\mathbf{x}), \dots, f_t(\mathbf{x})]^T \\ \quad = [1, x_1, \dots, x_p, x_1^2, \dots, x_1x_p, x_2^2, \dots, x_2x_p, x_p^2]^T \\ t = \frac{1}{2}(p+1)(p+2) \end{cases} \quad (3)$$

and the random function $z(\mathbf{x})$ is a stationary Gaussian process with zero mean and covariance:

$$\text{Cov}[z_l(\mathbf{x}), z_l(\mathbf{x}')] = \sigma_l^2 \mathcal{R}(\mathbf{x}, \mathbf{x}'), \quad l = 1, 2, \dots, q \quad (4)$$

where $\mathcal{R}(\mathbf{x}, \mathbf{x}')$ is the spatial correlation function between \mathbf{x} and \mathbf{x}' , and is also very critical for simulation accuracy. σ_l^2 is the process variance for the l th component of the response.

Several correlation functions are available in the literature, such as exponential, linear and Gaussian functions. The anisotropic Gaussian function is widely used for reliability problems [14]:

$$\mathcal{R}(\mathbf{x}, \mathbf{x}') = \prod_{l=1}^{p'} \exp(-\theta_l |\mathbf{x}_l - \mathbf{x}'_l|^2) \quad (5)$$

As shown by the above equations, Kriging model is completely defined by the vector of regression parameters β , the vector of correlation parameters θ and the stationary Gaussian process variance σ^2 .

For the set \mathbf{X} of design sites, we have the expanded $p' \times t$ design matrix \mathbf{F} , with $F_{kl} = f_l(\mathbf{x}_k)$,

$$\mathbf{F} = [f(\mathbf{x}_1), f(\mathbf{x}_2), \dots, f(\mathbf{x}_{p'})]^T \quad (6)$$

where $f(\mathbf{x})$ can be defined by Eq. (3).

Further, \mathbf{R} is the matrix of stochastic process correlation between design sites,:

$$R_{kl} = \mathcal{R}(\mathbf{x}_k, \mathbf{x}_l), \quad k, l = 1, 2, \dots, p' \quad (7)$$

The vector of correlations between design site and an untried point \mathbf{x} is:

$$\mathbf{r}(\mathbf{x}) = [\mathcal{R}(\mathbf{x}_1, \mathbf{x}), \mathcal{R}(\mathbf{x}_2, \mathbf{x}), \dots, \mathcal{R}(\mathbf{x}_{p'}, \mathbf{x})]^T \quad (8)$$

For a given sample of points, the vectors of regression parameter $\boldsymbol{\beta}$ and process variance σ^2 are obtained as the maximum likelihood estimate of a generalized least squares problem [15]:

$$\boldsymbol{\beta}^* = (\mathbf{F}^T \mathbf{R}^{-1} \mathbf{F})^{-1} \mathbf{F}^T \mathbf{R}^{-1} \mathbf{Y} \quad (9)$$

The maximum likelihood estimate of the variance is:

$$\sigma^{*2} = \frac{1}{p'} (\mathbf{Y} - \mathbf{F} \boldsymbol{\beta}^*)^T (\mathbf{Y} - \mathbf{F} \boldsymbol{\beta}^*) \quad (10)$$

Based on maximum likelihood estimation, the optimal coefficient θ^* of the correlation function are found [15]:

$$\theta^* = \min_{\theta} \{ \psi(\theta) \equiv |\mathbf{R}|_{p'}^{-1} \sigma^{*2} \} \quad (11)$$

where $|\mathbf{R}|$ is the determinant of \mathbf{R} .

Thus, the predicted response at given sample points \mathbf{x} is:

$$\hat{y}(\mathbf{x}) = \mathbf{f}(\mathbf{x})^T \boldsymbol{\beta}^* + \mathbf{r}(\mathbf{x})^T \mathbf{R}^{-1} (\mathbf{Y} - \mathbf{F} \boldsymbol{\beta}^*) \quad (12)$$

2.2. Distributed collaborative response surface method

In previous works, the distributed collaborative response surface method (DCRSM) has been introduced to improve numerical accuracy and computation efficiency [7, 10, 11]. In this paper, we apply DCRSM to carry out the probabilistic analysis of the fatigue performance for turbo-fan blades, considering relevant uncertainties.

In light of the interrelation between structural level responses, DCRSM can divide a multi-level nonlinear probability problem into several single-level probabilistic analyses which are solvable with limited computing resources. Following that, with respect to a specified failure criterion, the single-level results are combined to construct the global distributed collaborative regression model, in order to solve the complex nonlinear probability problem.

We assume Z and $\mathbf{X} = [x_1, x_2, \dots, x_n]$ ($x_i \sim N(\mu_{\theta}, \sigma_{\theta}^2)$) are the global output response and input variable vector of whole reliability analysis, and the given structure involves r failure modes with corresponding responses y_1, y_2, \dots, y_r , which are regarded as distributed output responses. The relationships between distributed output responses and corresponding input variables are treated as distributed response surface functions (DRSFs).

Based on the specified failure criterion, the global output response Z can be calculated as the function of the distributed output responses y_1, y_2, \dots, y_r :

$$Z = Z(\mathbf{y}) = Z(y_1, y_2, \dots, y_r) \quad (13)$$

Eq. (13) is called distributed collaborative response surface function (DCRSF).

2.3. Kriging-based distributed collaborative reliability approach

In previous works, the DRSFs of the DCRSM have been taken as quadratic polynomial functions, with limited precision in the output responses due to the limitation of quadratic polynomial functions in fitting RSFs. To solve this limitation of DCRSM, we integrate the Kriging regression model into DCRSM to develop the Kriging-based DCRSM.

For a complex probability problem involving l level interrelated responses, we assume that $\mathbf{y}^{(l)} (\mathbf{y}^{(l)} \in R^p)$ and $\mathbf{x}^{(l)} (\mathbf{x}^{(l)} \in R^n)$ denote the l th level structural output response and corresponding input variable vector, respectively. According to the principle of Kriging, the k th first-level output response $y_k^{(1)} (k = 1, 2, \dots, p_1)$ is expressed as:

$$y_k^{(1)} = \hat{y}(\mathbf{x}_k^{(1)}) = \mathbf{f}(\mathbf{x}_k^{(1)})^T \boldsymbol{\beta}_k^{(1)*} + \mathbf{r}(\mathbf{x}_k^{(1)})^T \mathbf{R}_k^{(1)-1} (\mathbf{Y}_k^{(1)} - \mathbf{F}_k^{(1)} \boldsymbol{\beta}_k^{(1)*}) \quad (14)$$

which is called first-level DRSF (DRSF-I) between the k th first-level output response $y_k^{(1)}$ and corresponding input variables. In the same way, all DRSFs-I can be established as the following vector form:

$$\mathbf{y}^{(1)} = (y_1^{(1)}, y_2^{(1)}, \dots, y_{p_1}^{(1)})^T \quad (15)$$

where p_1 is the number of first-level output responses.

Based on specified failure dependence, the first-level output responses $\mathbf{y}^{(1)}$ are regarded as the random variables of the second-level output responses $\mathbf{y}^{(2)}$. The s th second-level output response $y_s^{(2)}$ is expressed as:

$$y_s^{(2)} = \hat{y}(\mathbf{y}^{(1)}) = \mathbf{f}(\mathbf{y}^{(1)})^T \boldsymbol{\beta}_s^{(2)*} + \mathbf{r}(\mathbf{y}^{(1)})^T \mathbf{R}_s^{(2)-1} (\mathbf{Y}_s^{(2)} - \mathbf{F}_s^{(2)} \boldsymbol{\beta}_s^{(2)*}) \quad (16)$$

which is the second-level DRSF (DRSF-II).

In the same way, the relationships between the l th-level responses $\mathbf{y}^{(l)}$ and $(l-1)$ th-level responses $\mathbf{y}^{(l-1)}$ can be fitted. The r th output response of the l th-level responses $y_r^{(l)}$ can be expressed as:

$$y_r^{(l)} = \hat{y}(\mathbf{y}^{(l-1)}) = \mathbf{f}(\mathbf{y}^{(l-1)})^T \boldsymbol{\beta}_r^{(l)*} + \mathbf{r}(\mathbf{y}^{(l-1)})^T \mathbf{R}_r^{(l)-1} (\mathbf{Y}_r^{(l)} - \mathbf{F}_r^{(l)} \boldsymbol{\beta}_r^{(l)*}) \quad (17)$$

Finally, based on the specified failure criterion, the l th-level responses $\mathbf{y}^{(l)}$ are regarded as input variables of the global output response to model global DCRSF with Kriging:

$$Z = \hat{y}(\mathbf{y}^{(l)}) = \mathbf{f}(\mathbf{y}^{(l)})^T \boldsymbol{\beta}_Z^{(Z)*} + \mathbf{r}(\mathbf{y}^{(l)})^T \mathbf{R}_Z^{(Z)-1} (\mathbf{Y}_Z^{(Z)} - \mathbf{F}_Z^{(Z)} \boldsymbol{\beta}_Z^{(Z)*}) \quad (18)$$

which is the Kriging-based DCRSF.

Based on the mathematic model, the Kriging-based distributed collaborative reliability approach integrates the advantages of the Kriging and DCRSM. In view of the availability of the proposed Kriging-based DCRSM, it provides an enlightened insight for the reliability analysis and optimization design of complex mechanical structures. The proposed approach can be applied to improve the compu-

tational efficiency and numerical accuracy for the reliability analysis and optimization design of complex mechanical structures involving multi-failure modes and/or multi-component.

3. Reliability assessment framework with Kriging-based DCRSM: Case study

3.1. Deterministic analysis

3.1.1. Establishing Campbell diagram

A wide-chord turbo-fan blade without blade-root is selected as study object and meshed with hexahedral structured grids, consisting of 2784 nodes and 3596 elements. Titanium-alloy, with elastic modulus $E=112$ GPa, density $\rho=4453$ kg/m³ and Poisson ratio $\mu=0.32$, is chosen as the turbo-fan blade material, for which the finite element model (FEM) is established in Fig. 1.

To accomplish the vibration characteristics analysis, the turbo-fan blade FEM is fixed by constraining all degrees of freedom (DOFs) at the root and, then, modal analysis is carried out to acquire the first six-order natural frequencies under different rotational speeds, as shown in Table 1.

Generally, Campbell diagram aims at monitoring the dynamic process of rotor vibration characteristics with rotational speed, to determine the working state of the rotor in entire speed range, thus playing an important role in further analyzing the cause of abnormal fault

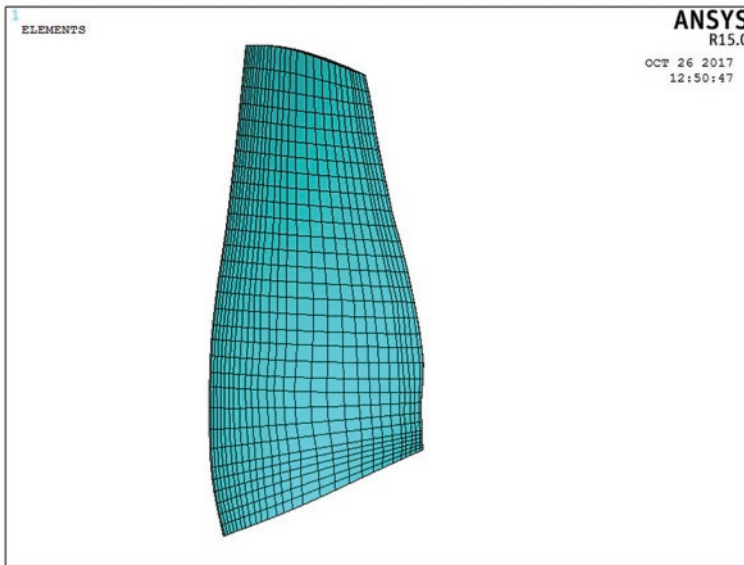


Fig. 1. Fan blade finite element model.

Table 1. The first six natural frequencies of the fan blade.

Rotational speed (rpm)	Frequencies (Hz)					
	1	2	3	4	5	6
0	60.611	189.29	423.85	471.59	675.97	810.85
1000	64.984	193.61	424.72	475.44	676.62	813.98
2000	76.136	205.97	427.04	486.87	678.48	823.08
3000	90.712	224.85	430.37	505.19	681.33	837.36
4000	106.58	248.33	434.46	528.99	684.89	855.66
5000	122.82	274.66	439.24	556.43	688.92	876.88
6000	139.10	302.45	444.73	585.52	693.36	900.40
7000	155.30	330.71	450.92	614.17	698.54	926.29

and the setting of limit amplitude. Based on the above modal analysis, a Campbell diagram is shown in Fig.2. In the Campbell diagram, the horizontal axis represents rotational speed ω and the vertical axis denotes structural frequency f . The black curves indicate the natural frequency versus the rotational speed of the blade with different modes, where the first six modes 1F, 2F, 1T, 3F, 2T and 2S represents first-order bending vibration, second-order bending vibration, first-order torsional vibration, third-order bending vibration, second-order torsional vibration and combined twisting vibration, respectively. The rays (colored lines) show different Engine order (E) lines. The engine

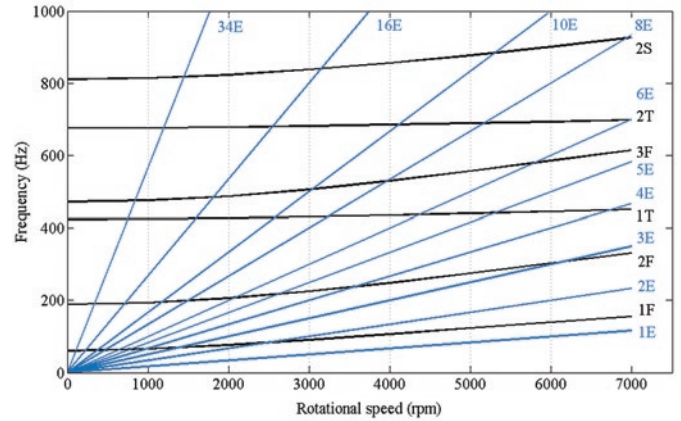


Fig. 2. Campbell diagram of the turbo-fan blade.

order excitation is a periodic force. The harmonics frequency depends on the rotational speed: $n \cdot E = n \cdot \omega / 60$, where n is the engine order. Also, the intersection between the n th engine order line and the line of natural frequencies of a mode is possible resonance point [8, 9].

From Table 1 and Fig. 2, we can see that the natural frequencies display a general trend of fluctuations: the frequencies gradually increase with the increasing modal order and rotational speed. As indicated in the Campbell diagram, before the idling rotation speed, rotational speed is usually shorter than transition speed, and destructive resonance is hardly caused. However, after the idling rotation speed, the engine turns into the normal working condition, and avoiding the speed of resonance is an effective approach to ensure the reliability of the fan blade.

3.1.2. Analyzing aerodynamic load

The influence of steady aerodynamic loads on the turbo-fan blade is analyzed by modelling real flow field at the rotational speed of 4150 rpm with the corresponding inlet and outlet boundary definition. The aerodynamic loads are mapped to the surface effect element of the fan blade to acquire equivalent stress distribution, as shown in Fig. 3. The fluid-structure interaction results illustrate that the most dangerous area of the blade is approximately located on the middle of suction surface, where the maximum equivalent stress $\sigma_{es,max}$ is 466.356 MPa with node 1522.

The dangerous area is the main concern to investigate the influence of the aerodynamic loads and rotational speed on the fatigue performance of the fan blade. Experimental evidence shows that resonance caused in the first three orders is the main failure form of rotor blades due to strong resonant energy. Therefore, the harmonic response

analysis without damping at the rotational speed of 4150 rpm, 83% of design speed, is performed to examine whether the first three-order modes are in a state of resonance, as shown in Fig. 4.

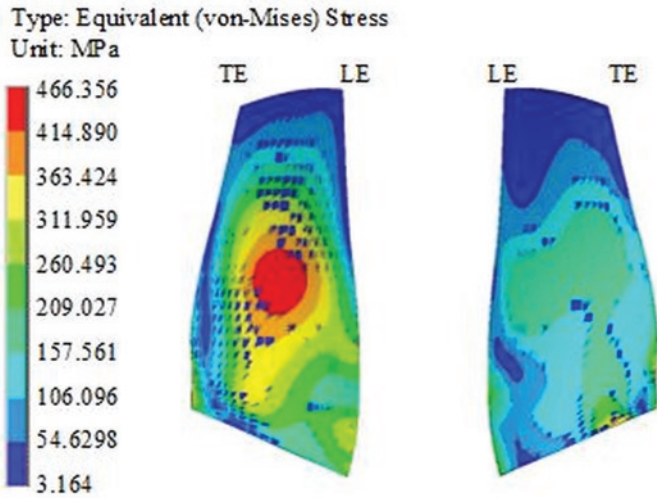


Fig. 3. Equivalent stress distribution of the fan blade: (left) suction surface and (right) pressure surface

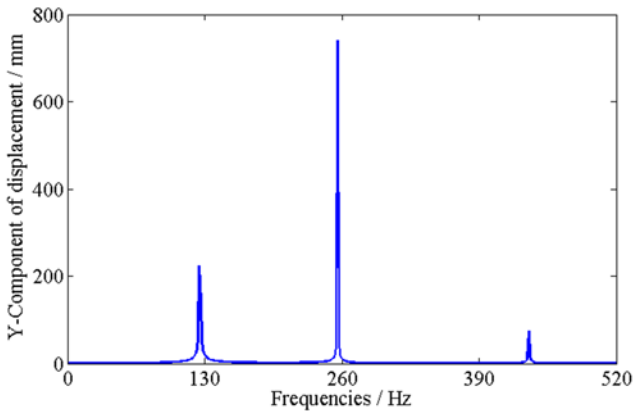


Fig. 4. Harmonic analysis result of the maximum stress node 1522

As indicated in Fig. 4, under aerodynamic load and centrifugal force, there are different degrees of resonance occurring for the fan blade in the first three-order modes. The corresponding resonance frequencies are $f_1=125.01\text{Hz}$, $f_2=256.59\text{ Hz}$ and $f_3=437.13\text{Hz}$, respectively, which are inconsistent with the first three natural frequencies of the turbo-fan blade under rotational speed, due to the influence of the aerodynamic load. In addition, the vibration amplitude without damping and actual situation are discrepant, therefore, Fig. 4 is only used to determine the resonant frequencies.

3.1.3. Calculating fatigue strength

In this sub-section, vibration stresses are calculated for the turbo-fan blade at the three resonant frequencies, based on the assumption that vibration stress mainly results from aerodynamic loads and centrifugal forces. Therefore, when the first three-order resonances simultaneously occur, the fatigue strength of the turbo-fan blade will reach the maximum value. Applying Eq. (19), the coupled harmonic response analysis is completed and the vibration stress of critical point 1522 can be acquired, as shown in Fig. 5. Fig. 5 shows the change of the vibration stress of node 1522 under three harmonic loads, and the maximum vibration stress $\sigma_{vs,max}$ reaches to 66.866 MPa.

$$\sigma_{vs} = \sigma_{es} \sin(2\pi \cdot f_1 \cdot t) + \sigma_{es} \sin(2\pi \cdot f_2 \cdot t) + \sigma_{es} \sin(2\pi \cdot f_3 \cdot t) \quad (19)$$

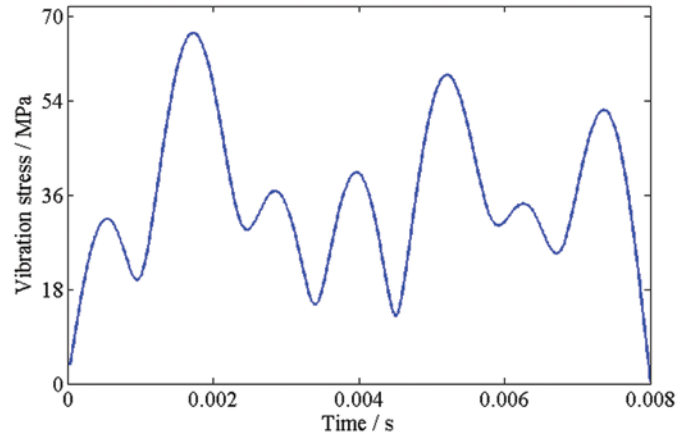


Fig. 5. Vibration stress of the maximum stress node 1522 under three harmonic loads

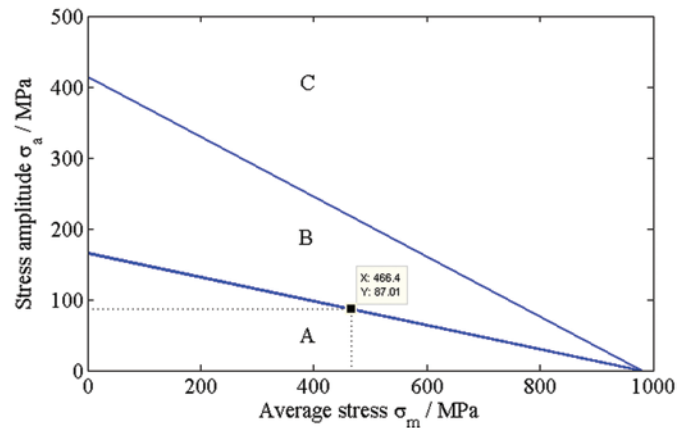


Fig. 6. Modified Goodman curve with titanium-alloy

Goodman curve has been widely applied in structural fatigue strength design, by taking into account the fatigue stress amplitude, average stress, material properties factors. Based on the yield limit and the linear empirical formula proposed by Goodman, the modified Goodman curve has been obtained, replacing actual fatigue limit line with a straight line [12]. In order to check the vibration condition of the turbo-fan blade at the working point, the modified Goodman curve with titanium-alloy is made, as shown in Fig. 6, where regions A, B and C represent safe, unsafe and damage regions against vibration, respectively. Therefore, the vibration stress of the turbo-fan blade should be limited to region A, and the limit equation between average stress σ_m and stress amplitude σ_a corresponding to region A can be fitted:

$$\sigma_a = -0.1693 \cdot \sigma_m + 166 \quad (20)$$

From Fig. 6 and Eq. (20), when the maximum working stress $\sigma_{es,max}$ is 466.356 MPa, the corresponding maximum vibration stress is $\sigma_a=87.01\text{ MPa}$. Since the maximum vibration stress $\sigma_{vs,max}=66.866\text{ MPa}$ is less than 87.01 MPa, thus, the turbo-fan blade is safe under the three harmonic loads.

3.2. Reliability analysis framework

From the deterministic analyses, it is obvious that the fatigue strength prediction for the turbo-fan blade is a multi-level problem. In order to improve numerical accuracy and computational efficiency, we integrate parallel computation into the proposed Kriging-based DCRSM to perform the fatigue strength reliability assessment of the turbo-fan blade.

In this paper, the fatigue strength of the turbo-fan blade is regarded as the global output response. The elastic modulus E , density ρ , Poisson ratio μ are considered as random input variables, and coefficients of variation are set to 0.02. The first three-order resonant frequencies are regarded as the distributed output responses. Based on the basic principle of Kriging-based DCRSM, the statistical characteristics of the first three resonant frequencies are acquired, and then, the fatigue strength $\sigma_{vs,max}$ is solved, considering the random input variables and resonant frequencies.

Eq. (19) indicates the global DCRSF for resolving the fatigue strength of the turbo-fan blade. In the light of the basic principle of the Kriging-based DCRSM, we extend the Kriging-based DCRSM together with the global DCRSF to clearly describe the proposed method.

In this paper, random variables $\mathbf{x} = (E, \rho, \mu)$ are regarded as the input variables of the first three-order resonant frequencies f_1, f_2 and f_3 . Based on Kriging regression, the DRSFs can be shown Eq. (21):

$$f_i = \hat{y}(\mathbf{x}) = \mathbf{f}_i(\mathbf{x})^T \boldsymbol{\beta}_i^* + \mathbf{r}_i(\mathbf{x})^T \mathbf{R}_i^{-1} (\mathbf{Y}_i - \mathbf{F}_i \boldsymbol{\beta}_i^*), \quad i = 1, 2, 3 \quad (21)$$

Then, the first three-order resonant frequencies f_1, f_2 and f_3 are considered as basic input variables of the fatigue strength $\sigma_{vs,max}$ of the turbo-fan blade. The DCRSF can be expressed:

$$\sigma_{vs,max} = \mathbf{g}(E, \rho, \mu, f_1, f_2, f_3) = \left[\sum_{i=1}^3 \sigma_{es} \cdot \sin(2\pi \cdot f_i \cdot t) \right]_{max} \quad (22)$$

The limit state function is defined as follows:

$$Z = \hat{\sigma}_a - \sigma_{vs,max} \quad (23)$$

in which $Z \geq 0$ denotes that the structure is safe, while $Z < 0$ denotes that the structure is out of order.

Subsequently, the structural failure probability can be estimated by:

$$\hat{P}_f = \frac{1}{M} \sum_{j=1}^M I_F [Z_j] = \frac{m}{M} \quad (24)$$

$$I_F [Z_j] = \begin{cases} 1, & Z < 0 \\ 0, & Z \geq 0 \end{cases} \quad (25)$$

where $I_F [\cdot]$ is the indicator function in the failure domain, m the number of sample points in the failure domain, and M the number of total sample points Z .

Thus, the structural reliability R can be estimated by:

$$R = 1 - \hat{P}_f \quad (26)$$

Finally, the structural sensitivity analyses including sensitivity and normalized significance are performed by Eq. (27) and Eq. (28):

$$\beta_{y_i} = \frac{\partial g_Y(\mathbf{y})}{\partial y_i} \sigma_{y_i} \quad (27)$$

$$\alpha_{y_i}^2 = \left[\frac{\partial g_Y(\mathbf{y})}{\partial y_i} \sigma_{y_i} \right]^2 / \left[\sum_{i=1}^6 \left[\frac{\partial g_Y(\mathbf{y})}{\partial y_i} \sigma_{y_i} \right]^2 \right], \sum_{i=1}^6 \alpha_{y_i}^2 = 1 \quad (28)$$

where $\mathbf{y} = (E, \rho, \mu, f_1, f_2, f_3)$ and α_{y_i} is sensitivity coefficient. In addition, the higher the sensitivity index $\alpha_{y_i}^2$, the more important the corresponding parameter y_i is.

Table 2. Statistical characteristics of the three orders natural frequencies (Hz)

Frequency	Mean	Std. Dev.	Skew.Coeff.	Kurt.Coeff.	Min. value	Max. value
f_1	125.01	1.4689	0.0042606	-2202.1	119.97	130.34
f_2	256.17	2.9648	0.015865	-2211.2	245.03	267.04
f_3	437.18	5.9076	0.045818	-2262.4	414.58	461.98

4. Fatigue strength reliability assessment of turbo-fan blades

4.1. Probabilistic analysis of natural frequency

Twelve harmonic response analyses are performed by MCM with Latin hypercube sampling and, then, the Kriging model is constructed to obtain 10000 sets of resonant frequencies. The statistical characteristics of the first three order resonant frequencies are obtained. Fig. 7, Fig. 8 and Fig. 9 show that the sampling histories and distribution histogram of the first three-order resonant frequencies, respectively. Table 2 lists their statistical characteristics. It can be seen that the first

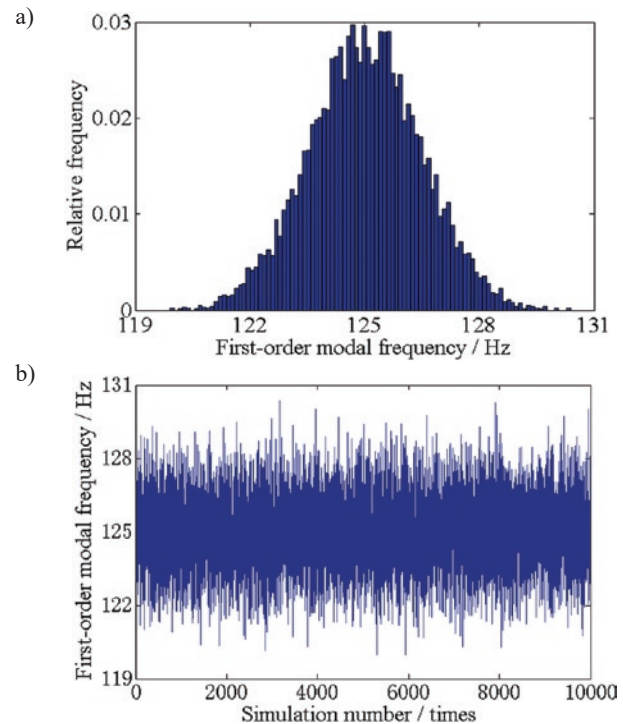


Fig. 7. First-order resonant frequency distribution: (a) distribution histogram and (b) sampling history

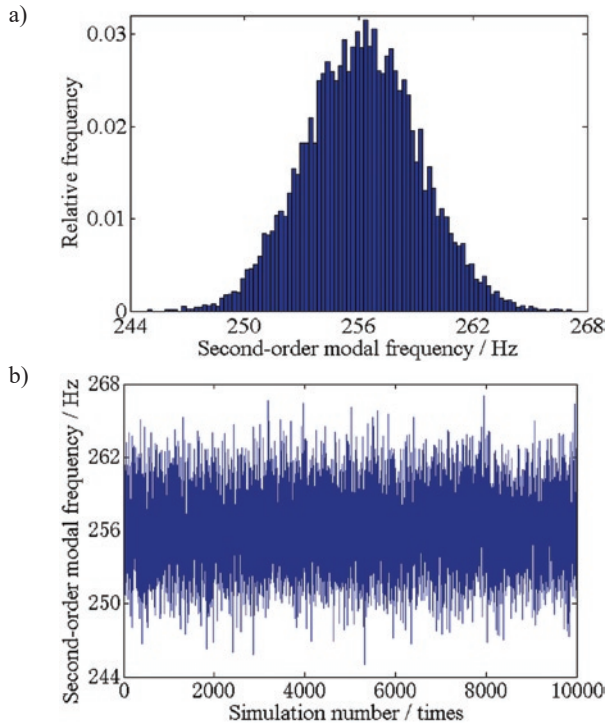


Fig. 8. Second-order resonant frequency distribution: (a) distribution histogram and (b) sampling history

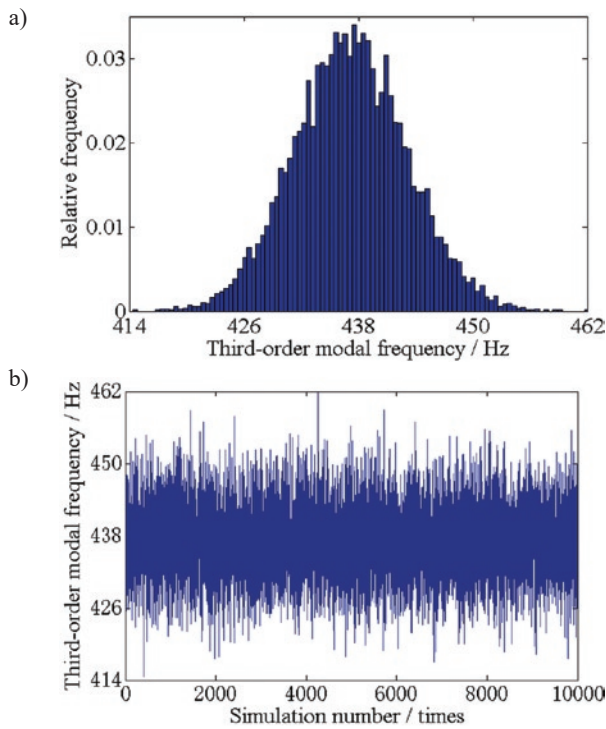


Fig. 9. Third-order resonant frequency distribution: (a) distribution histogram and (b) sampling history

three-order resonant frequencies follow normal distributions, with content prediction results.

4.2. Fatigue strength reliability analysis

In this sub-section, the distributed responses, first-order frequency f_1 , second-order frequency f_2 and third-order frequency f_3 , and the

material properties, elastic modulus E , density ρ and Poisson ratio μ are considered as the basic input variables of the fatigue strength response model. Considering their randomness, the three harmonic loads interaction analyses under the three-order resonant frequencies are performed and the maximum vibration stress $\sigma_{vs,max}$ of the most dangerous point is acquired to extract 10000 samples and their statis-

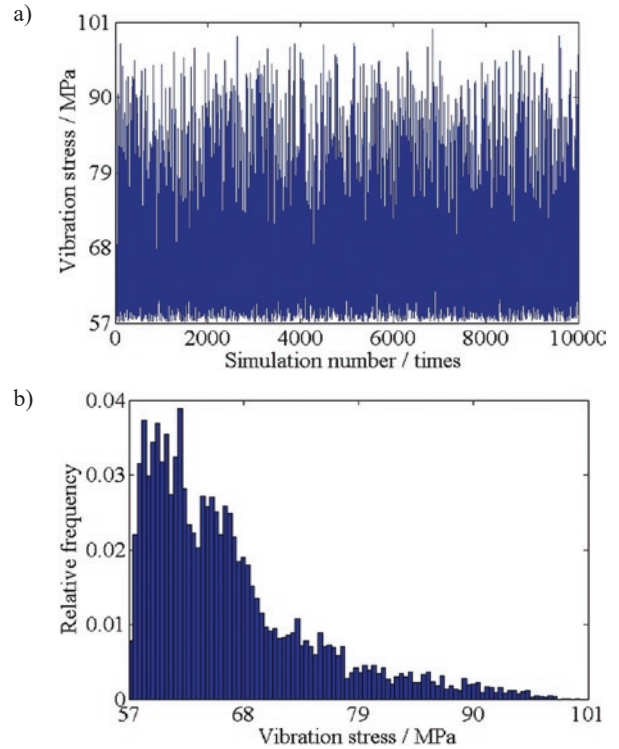


Fig. 10. Fatigue strength probability distribution: (a) sampling history and (b) distribution histogram

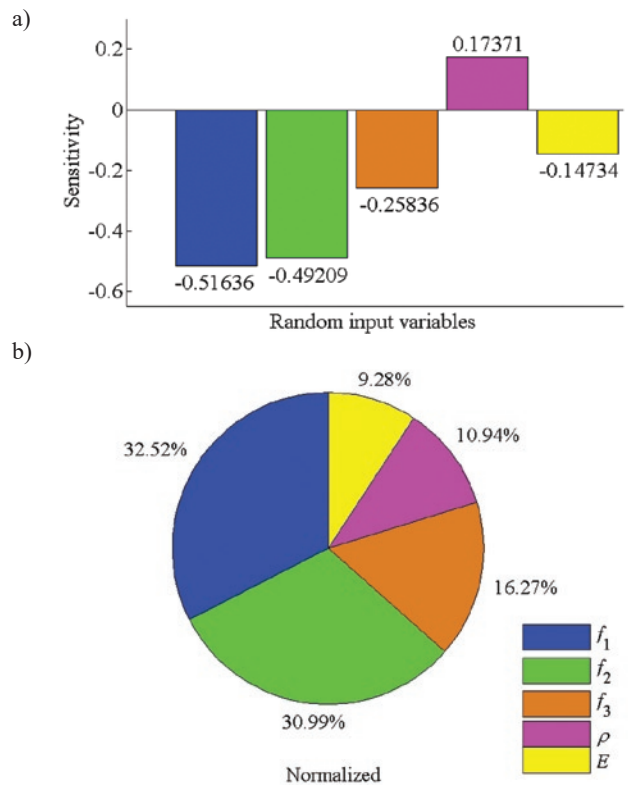


Fig. 11. Sensitivity and normalized significance of relevant

Table 3. Statistical characteristics of fatigue strength and reliability

Mean (MPa)	Std. Dev. (MPa)	Min. (MPa)	Max. (MPa)
66.567	8.0006	57.133	99.976

tical characteristics. Fig. 10 and Table 3 show that the probabilistic distribution of the vibration stress $\sigma_{vs,max}$. Based on the modified Goodman curve in Fig. 6, the fatigue strength reliability of the turbo-fan blade is found to be 96.808%, with confidence level of 0.95.

4.3. Sensitivity analysis

Sensitivity analysis is performed to evaluate which variables have greater influence on the output response, and further guide the structural design. In this sub-section, sensitivity analysis has been completed to investigate the influence of random variables $y = (E, \rho, \mu, f_1, f_2, f_3)$ on the fatigue strength with significance level of 2.5%. The sensitivity and normalized significance are shown in Fig. 11.

From Fig. 11, we can see that the first three-order resonant frequencies have great impact on the fatigue strength of the turbo-fan blade, and negative sensitivity indicates that the fatigue strength reduces with increasing resonant frequency. In addition, the influences of natural frequencies with different modes on the fatigue strength greatly varies and the normalized significance of the first-order, second-order and third-order resonant frequencies on the fatigue strength decrease in order. Also, the first-order resonant frequency has the greatest effect on the fatigue strength of the turbo-fan blade. Therefore, the first-order resonant frequency should be given sufficient attention in the initial design of the turbo-fan blade.

References

1. Beck J L, Au S K. Bayesian updating of structural models and reliability using Markov chain Monte Carlo simulation. *Journal of Engineering Mechanics* 2002; 128(4): 380-391, [https://doi.org/10.1061/\(ASCE\)0733-9399\(2002\)128:4\(380\)](https://doi.org/10.1061/(ASCE)0733-9399(2002)128:4(380)).
2. Billinton R, Wang P. Teaching distribution system reliability evaluation using Monte Carlo simulation. *IEEE Transactions on Power Systems* 1999; 14(2): 397-403, <https://doi.org/10.1109/59.761856>.
3. Bucher C G, Bourgund U. A fast and efficient response surface approach for structural reliability problems. *Structural Safety* 1990; 7(1): 57-66, [https://doi.org/10.1016/0167-4730\(90\)90012-E](https://doi.org/10.1016/0167-4730(90)90012-E).
4. Cornell C A. A first order reliability theory of structural designs. *Structural Reliability and Codified Design*, 1970.
5. Das P K, Zheng Y. Cumulative formation of response surface and its use in reliability analysis. *Probabilistic Engineering Mechanics* 2000; 15(4): 309-315, [https://doi.org/10.1016/S0266-8920\(99\)00030-2](https://doi.org/10.1016/S0266-8920(99)00030-2).
6. Der Kiureghian A, Lin H Z, Hwang S J. Second-order reliability approximations. *Journal of Engineering mechanics* 1987; 113(8): 1208-1225, [https://doi.org/10.1061/\(ASCE\)0733-9399\(1987\)113:8\(1208\)](https://doi.org/10.1061/(ASCE)0733-9399(1987)113:8(1208)).
7. Gao H F, Bai G C, Gao Y, Bao T W. Reliability analysis for aeroengine turbine disc fatigue life with multiple random variables based on distributed collaborative response surface method. *Journal of Central South University* 2015; 22(12): 4693-4701, <https://doi.org/10.1007/s11771-015-3020-x>.
8. Gao H, Bai G. Reliability analysis on resonance for low-pressure compressor rotor blade based on least squares support vector machine with leave-one-out cross-validation. *Advances in Mechanical Engineering* 2015; 7(4): 1687814015578351, <https://doi.org/10.1177/1687814015578351>.
9. Gao H F, Bai G C. Vibration reliability analysis for aeroengine compressor blade based on support vector machine response surface method. *Journal of Central South University* 2015; 22(5): 1685-1694, <https://doi.org/10.1007/s11771-015-2687-3>.
10. Gao H, Fei C, Bai G, Ding L. Reliability-based low-cycle fatigue damage analysis for turbine blade with thermo-structural interaction. *Aerospace Science and Technology* 2016; 49:289-300, <https://doi.org/10.1016/j.ast.2015.12.017>.
11. Gao H, Wang A, Bai G, Wei C, Fei C. Substructure-based distributed collaborative probabilistic analysis method for low-cycle fatigue damage assessment of turbine blade-disk. *Aerospace Science and Technology* 2018; 79: 636-646, <https://doi.org/10.1016/j.ast.2018.06.023>.
12. Goodman J. *Mechanics applied to engineering*. Green: Longmans, 1918.
13. Hasofer A M, Lind N C. Exact and invariant second-moment code format. *Journal of the Engineering Mechanics Division* 1974; 100(1): 111-121.
14. Isaaks E H, Srivastava R M. *An introduction to applied geostatistics* (No. BOOK). Oxford University Press, 1989.
15. Lophaven S N, Nielsen H B, Sondergaard J, DACE-A M K T. *Informatics and mathematical modelling*. Technical University of Denmark, 2002.
16. Poursaeidi E, Babaei A, Arhani M M, Arablu M. Effects of natural frequencies on the failure of R1 compressor blades. *Engineering Failure Analysis* 2012; 25: 304-315, <https://doi.org/10.1016/j.engfailanal.2012.05.013>.

5. Conclusions

In this paper, a reliability approach, integration of the Kriging and distributed collaborative response surface method (DCRSM), is proposed for the fatigue strength reliability analysis of turbo-fan blades. In order to determine the probable resonance points within the entire design speed range, the Campbell diagram of a turbo-fan blade is used. The aerodynamic pressure is exerted onto the surface of the turbo-fan blade to implement the harmonic analysis under fluid-structure interaction and solve the first three-order resonance frequencies for the fan blade. Also, a coupling harmonic response analysis is performed based on the assumption that the vibration stress mainly results from aerodynamic loads. Based on modified Goodman curve with titanium-alloy, the fatigue strength is predicted for the fan blade. Based on the above analyses, a reliability assessment framework is presented with Kriging-based DCRSM.

Considering the relevant uncertainties, the reliability assessment of the fatigue strength for the turbo-fan blade is launched. Applying Kriging regression model, first three-order resonance frequency samples are generated. Then, the frequencies and material properties are considered as input variables to extract the fatigue strength samples and statistical characteristics. Finally, the fatigue strength reliability assessment and sensitivity analysis are performed for the turbo-fan blade. The results show that the first three-order resonant frequencies have important and negative influence on the vibration stress.

Acknowledgements

This paper is co-supported by the National Natural Science Foundation of China (Grant no. 51705309), and China Postdoctoral Science Foundation (Grant no. 2017M621481). All authors would like to thank them.

17. Rackwitz R, Flessler B. Structural reliability under combined random load sequences. *Computers & Structures* 1978; 9(5): 489-494, [https://doi.org/10.1016/0045-7949\(78\)90046-9](https://doi.org/10.1016/0045-7949(78)90046-9).
18. Rajashekhar M R, Ellingwood B R. A new look at the response surface approach for reliability analysis. *Structural Safety* 1993; 12(3): 205-220, [https://doi.org/10.1016/0167-4730\(93\)90003-J](https://doi.org/10.1016/0167-4730(93)90003-J).
19. Sacks J, Welch W J, Mitchell T J, Wynn H P. Design and analysis of computer experiments. *Statistical Science* 1989; 409-423, <https://doi.org/10.1214/ss/1177012413>.
20. Srinivasan A V. Flutter and resonant vibration characteristics of engine blades. *Journal of Engineering for Gas Turbines and Power* 1997; 119(4): 742-775, <https://doi.org/10.1115/1.2817053>.
21. Subrahmanyam K B, Kulkarni S V, Rao J S. Coupled bending-bending vibrations of pre-twisted cantilever blading allowing for shear deflection and rotary inertia by the Reissner method. *International Journal of Mechanical Sciences* 1981; 23(9): 517-530, [https://doi.org/10.1016/0020-7403\(81\)90058-8](https://doi.org/10.1016/0020-7403(81)90058-8).
22. Tvedt L. Distribution of quadratic forms in normal space-application to structural reliability. *Journal of Engineering Mechanics* 1990; 116(6): 1183-1197, [https://doi.org/10.1061/\(ASCE\)0733-9399\(1990\)116:6\(1183\)](https://doi.org/10.1061/(ASCE)0733-9399(1990)116:6(1183)).

Hai-Feng GAO

School of Mechanical Engineering
Shanghai Jiao Tong University
Shanghai, China
Energy Department, Politecnico di Milano
Milano, Italy

Anjenq WANG

School of Mechanical Engineering
Shanghai Jiao Tong University
Shanghai, China.

Enrico ZIO

Energy Department, Politecnico di Milano
Milano, Italy
MINES ParisTech, PSL Research University, CRC
Sophia Antipolis, France
Department of Nuclear Engineering, College of Engineering,
Kyung Hee University, Korea

Wei MA

School of Aeronautics and Astronautics
Shanghai Jiao Tong University
Shanghai, China

E-mails: ghf121117@126.com, aj.wang@sjtu.edu.cn,
enrico.zio@polimi.it, mawei@sjtu.edu.cn
